

A comparative study of Sparse and Tikhonov regularization methods in the gravity inversion: a case study of manganese deposit in Iran

Bardiya Sadraeifar ^a, Maysam Abedi ^{b, *}

^a *Institute of Geophysics, University of Tehran, Iran.*

^b *School of Mining Engineering, Faculty of Engineering, University of Tehran, Iran.*

Article History:

Received: 22 November 2023.

Revised: 28 December 2023.

Accepted: 09 January 2024.

ABSTRACT

The gravity inversion methods play a fundamental role in subsurface exploration, facilitating the characterization of geological structures and economic deposits. In this study, we conduct a comparative analysis of two widely used regularization methods, Tikhonov (L_2) and Sparse (L_1) regularization, within the framework of the gravity inversion. To assess their performance, we constructed two distinct synthetic models by implementing tensor meshes, considering station spacing to discretize the subsurface environment precisely. Both methods have proven ability to recover density distributions, while minimizing the inherent non-uniqueness and ill-posed nature of the gravity inversion problems. The Tikhonov regularization yields stable results, presenting smooth model parameters even with limited prior information and noisy data. Conversely, the Sparse regularization, utilizing sparsity-promoting penalties, excels in capturing sharp geological features and identifying anomalous regions, such as mineralized zones. Applying these methodologies to real gravity data from the Safu manganese deposit in northwest Iran, we assess their efficacy in recovering the geometry of dense ore deposits. The Sparse regularization demonstrates superior performance, yielding lower misfit values and sharper boundaries during individual inversions. This underscores its capacity to provide a more accurate representation of the depth and edges of anomalous targets in this specific case. However, both methods represent the same top depth of the target in the real case study, but the lower depth and density distribution were not the same in the XZ cross-sections. The inversion results imply the presence of a near-surface deposit characterized by a high-density contrast and linear distribution, attributed to the high grade of manganese mineralization.

Keywords: *Tikhonov regularization, Sparse regularization, Synthetic models, Tensor meshes, Mineralized zones, Manganese deposit.*

1. Introduction

Geophysics stands as a discipline where mathematical methodologies have played a central role for over a century. The exploration of geophysical challenges has resulted in the formulation of numerous mathematical models, showcasing their successful application not only within Earth sciences but also across various domains. The evolution of diverse geophysical research methods has led to the establishment of the theory of inverse problems. Subsequently, methodologies and algorithms have been devised to address predominantly ill-posed problems associated with these inverse challenges [1].

Regularization and optimization are fundamental mathematical techniques in geophysics, specifically within the context of the inversion process designed to unveil subsurface properties and Earth's geological features. These methods address the inherent non-uniqueness and ill-posed nature of inverse problems. Optimization involves determining optimal model parameters aligned with available data, while conforming to specific regularization constraints. Regularization methods are crucial for incorporating prior information and assumptions into inverse problem solutions, effectively acting as constraints on the recovered models [2]. The choice of regularization parameters and methods significantly influences the trade-off between fitting observed data. In the realm of inverse problems, where achieving a desired tolerance can yield various fitting models, the key task is selecting a model that aligns

with both observed data and prior knowledge [3]. Regularization emerges as a central player in this process, guiding the model selection journey by applying norms to assess the size or complexity of each model. The ultimate goal is to formulate a relevant regularization term encompassing prior insights, penalizing specific model traits, such as deviations from a reference model or variations in spatial derivatives. Minimizing this regularization term during the optimization phase ensures the identification of a model adept at fitting the data and conforming to anticipated characteristics, effectively mitigating the inherent non-uniqueness in inverse problems [3].

The majority of subsurface geological features exhibit a smooth and sharp structure, requiring the application of suitable regularization methods to address this challenge. However, it is essential to note that the selection of regularization methods depends on the inversion goals and the specific geological features encountered. Stratigraphic layers and geological boundaries typify smooth geological structures, while faults, karst formations, ore deposits, and volcanic structures represent sharp geological features. In this review, we provide a brief overview of the primary regularization methods commonly employed in the geophysical inversion process and explore their applications.

Regularization, also known as damping, plays an essential role in specific applications within the field of inverse problems [4]. The first

* Corresponding author. *E-mail address:* maysamabedi@ut.ac.ir (M. Abedi).

application is the stabilization of solutions [5]. Ill-posed inverse problems typically yield infinitely many solutions, rendering them sensitive to noise in the data. Regularization introduces a controlled level of smoothness or sparsity into the solutions, ensuring stability and preventing the amplification of noise [6]. Another crucial application involves balancing data fidelity [5]. Regularization strikes a balance between fitting the observed data and maintaining the smoothness or sparsity of the model [7]. It introduces a penalty term that discourages overly complex or noisy solutions, while ensuring the model remains consistent with the measurements [6]. The third application is about dealing with non-uniqueness. Ill-posed problems often admit multiple possible solutions that can equally fit the data. Regularization assists in narrowing down the range of acceptable solutions by favoring those that align with the regularization constraints [8]. This not only enhances the reliability of the inversion results but also makes them more interpretable.

The Tikhonov regularization, a widely used method, was developed by Tikhonov and Arsenin back in 1977 [8]. It brings in a penalty term to strike a balance between fitting the observed data and controlling the complexity of the model [1]. This regularization encourages a solution with smaller parameter values, effectively favoring a smoother and more stable solution. It helps mitigate the effects of noise in the data and prevents overfitting [9]. This approach promotes smoothness in the reconstructed model during inversion and is especially well-suited for scenarios where we anticipate gradual changes in physical properties. The Tikhonov regularization is commonly used in seismic exploration. Seismic data often suffer from blurring effects and noise during acquisition. The Tikhonov regularization helps in deblurring seismic images and suppressing noise by introducing a regularization term that penalizes overly complex or oscillatory solutions [10].

Another regularization method is the Sparsity regularization. This method adds a penalty term (in this study, the penalty term is based on the L_1 norm) based on the absolute values of model parameters. It encourages sparsity in the solution, making some parameters exactly zero [11]. In other words, it selects solutions with the minimum number of non-zero model parameters. In geological conditions, where the true subsurface model may have a few significant features surrounded by a more homogeneous background, sparsity regularization can help identify and recover these significant features [12]. Recent findings indicate that sparse solutions frequently provide more accurate representations of real objects compared to solutions characterized by the L_2 norm [12].

Then, there is the Total Variation regularization, occasionally known as TV denoising, which plays a significant role in seismic and electromagnetic imaging. It excels at enhancing the resolution and quality of results when dealing with noisy data [13-16]. This method finds solutions that are mostly smooth but allow for sudden changes in certain regions. This is really useful in geophysics when we want to find regions where physical properties, including density or conductivity change quickly. Denoising is a type of the linear inverse problem, aiming to remove noise from a signal or image, while maintaining the overall structure of the original content. In the image processing, the assessment of the resulting model's quality is often subjective and depends on specific criteria or motivations [5].

Lastly, we have the Bayesian Regularization, a method that enables geophysicists to incorporate prior geological knowledge and constraints into the inversion process, leading to improved accuracy and result reliability [17, 18]. In this approach, the model is considered a random variable, and we aim to estimate its probability distribution. By combining a prior distribution for the model parameters with the available data, we obtain a posterior distribution for the model parameters. It is noteworthy that in certain scenarios, the Bayesian approach yields solutions equivalent to those obtained through least squares, maximum likelihood, and the Tikhonov regularization methods [5].

Due to the significant exploratory relevance of the Safu site and the availability of reliable gravity data, numerous noteworthy research studies have been conducted on it. In 2014, Vatankhah et al. undertook research employing the Tikhonov regularization with the minimum

support stabilizer for the underdetermined 2D inversion of the gravity data [19]. In 2021, Varfinezhad and Ardestani conducted research on the gravity inversion, incorporating depth weighting and compactness constraints [20]. In this study, we conduct a gravity inversion employing the Sparse regularization, with the primary goal of promoting sparsity in the recovered model. This approach utilizes the iteratively reweighted least squares (IRLS) method to dynamically adjust the trade-off between data misfit and regularization throughout the inversion process. Additionally, we perform a gravity inversion using the Tikhonov regularization, with the objective of obtaining a model that strikes a balance between data misfit and smoothness. The efficiency of both inversion methods is assessed in terms of recovering the geometry and depth of a dense ore deposit. Despite dealing with a near-surface target, distinct results emerge from these methods, providing valuable insights into the selection of regularization techniques for shallow exploratory targets.

For geophysical data processing, we utilized the simPEG library [21], version 0.20 within the Python programming language. The properties of operating system for forward and inverse modelling are an ASUS laptop with an AMD A6 3.4 GHz CPU with 8G Ram.

2. Methodology

2.1. Meshing

Choosing a suitable discretization plays a fundamental role in computational modelling and simulations, covering various scientific domains, including geophysics. This essential technique involves the creation of a grid or mesh that discretizes the subsurface environment into more manageable elements [21]. In the field of geophysics, accurate meshing plays an important role in the numerical modelling and simulation of subsurface structures and natural phenomena. Employing a fine mesh, which takes into account the intervals between data points, results in a more accurate representation of the subsurface compared to using a coarse mesh. Tensor meshing, a specialized method within meshing, comes into focus when addressing complex geological formations and anisotropic properties, allowing for the creation of finer cells [21]. Figure 1 shows how the choice between a coarse mesh (1b) and a fine mesh (1c) impacts the recovery of a synthetic cube. The illustration highlights that fine tensor meshes work better at capturing the edges of the cube compared to coarse meshes. The density contrast of the cube in the true model was considered as 1.5 gr/cm^3 and for the background as 0 gr/cm^3 . It is evident that a more precise recovery of density and geometry is achieved under the second condition.

2.2. Forward Modelling

In both synthetic and real cases, the model space is characterized by a tensor mesh. The predicted data is obtained by summing the gravity effects of individual cells at each gravity measurement point on the ground surface [22]. This process is generally represented as follows:

$$F(\mathbf{m}_{grav}) = \mathbf{d}_{pred} \quad (1)$$

The forward operator F acts on the subsurface model, \mathbf{m}_{grav} , computing the sum of gravity effects exerted by individual cells within the model at each gravity measurement point on the ground surface. The outcome, \mathbf{d}_{pred} , represents the predicted gravity data.

The gravitational effect of each cell within the tensor mesh is calculated using the below equation, representing a detailed form of Eq.1 [23, 24]:

$$F(\mathbf{m}_{grav}) = G\rho \sum_{i=1}^2 \sum_{j=1}^2 \sum_{k=1}^2 \mu_{ijk} \left[z_k \arctan \frac{x_i y_i}{z_k R_{ijk}} - x_i \log(R_{ijk} + y_i) - y_i \log(R_{ijk} + x_i) \right] \quad (2)$$

And:

$$R_{ijk} = \sqrt{x_i^2 + y_j^2 + z_k^2} \quad (3)$$

$$\mu_{ijk} = (-1)^i (-1)^j (-1)^k \quad (4)$$

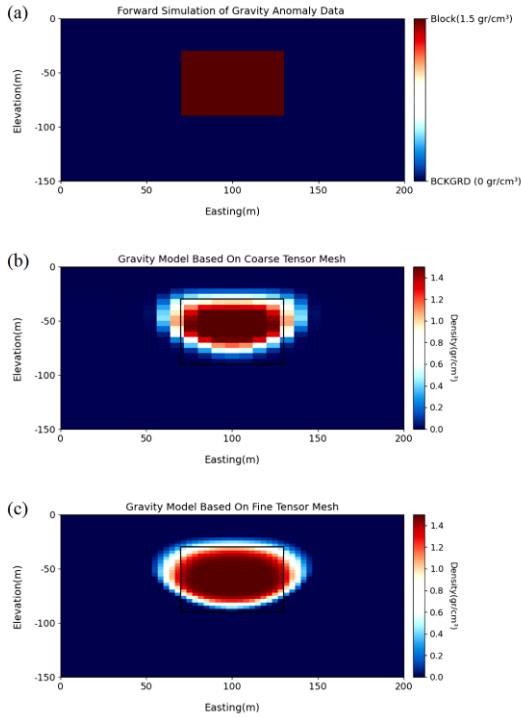


Figure 1. Illustrating the results of inverting simple geometrical shape using various mesh sizes, (a) True Model, (b) Reconstruction of a geometrical shape with a coarse tensor mesh, (c) Reconstruction of a geometrical shape with a fine tensor mesh.

Where G represents the universal gravitational constant and ρ denotes the density. z_k , x_i and y_i represent the vertical coordinate of the cell center, and the horizontal coordinates of the observation point. R_{ijk} represents the radial distance from the cell center to the observation point. This equation (2) calculates the gravitational effect of each cell in a discretized 3D subsurface model on the observation point. It considers the geometric factors and distances between the cell center and the observation point, incorporating the density distribution within the model. The alternating signs in the coefficient μ_{ijk} account for the arrangement of cells in the 3D model. The triple summation ensures that the contribution of each cell in the model is considered.

2.3. Inversion Methodology

The theoretical basis of the inversion methodology utilized in the SimPEG framework finds its roots in the works of Li and Oldenburg [25] and Oldenburg and Li [26]. In this section, we provide a brief summary of the employed inversion methodology. After introducing the generalized form of inversion, our focus shifts to the exploration of diverse regularization terms incorporated into the objective functions. The inversion is frequently conceptualized as an optimization problem in the following form [25]:

$$\min \phi(m) = \phi_d + \beta \phi_m. \quad (5)$$

The misfit function, denoted as ϕ_d and expressed in Eq.6, serves to quantify the disparity between observed data (\mathbf{d}^{obs}) and predicted data (\mathbf{d}^{pred}), with σ representing the estimated uncertainties in the data [25].

$$\phi_d = \sum_{i=1}^N \left(\frac{d_i^{pred} - d_i^{obs}}{\sigma_i} \right)^2 \quad (6)$$

ularization function, represented by ϕ_m , introduces prior information to address the non-uniqueness inherent in the inverse problem, enhancing its solution. β controls the balance between misfit and regularization [26]. The key distinction between two inversions lies in their regularization terms. The Tikhonov regularization is formulated in Eq.7:

$$\phi_{m_{Tikhonov}} = \alpha_s \phi_s + \alpha_x \phi_x + \alpha_y \phi_y + \alpha_z \phi_z = \sum_{r=s,x,y,z} \alpha_r \|\mathbf{W}_r \mathbf{V}_r \mathbf{G}_r (\mathbf{m} - \mathbf{m}^{ref})\|_2^2. \quad (7)$$

In Eq. (7), ϕ_s quantifies the deviation of the discrete model (\mathbf{m}) from a reference model (\mathbf{m}^{ref}), whereas ϕ_x , ϕ_y , and ϕ_z gauge the model's roughness. The coefficients α_s , α_x , α_y , and α_z govern the proximity of the derived model to the reference model and the flatness of the resulting model, respectively [26]. \mathbf{V} represents the discrete volume elements. The matrices \mathbf{G}_x , \mathbf{G}_y , and \mathbf{G}_z denote discrete gradient operators. In the context of the smallness component, \mathbf{G}_s simplifies to the identity matrix. \mathbf{W}_s denotes the weight for the smallest model and \mathbf{W}_x , \mathbf{W}_y , and \mathbf{W}_z denote the weights for model flatness in three Cartesian coordinates [25]. \mathbf{m} represents the model vector, which is the unknown subsurface property that the inversion is trying to recover. \mathbf{m}^{ref} represents a reference model or a prior estimate of the subsurface properties. It is incorporated into the inversion process to provide additional information and constraints [25]. The sparsity regularization term is represented as follows:

$$\phi_{m_{sparse}} = \sum_{r=s,x,y,z} \alpha_r \|\mathbf{W}_r \mathbf{V}_r \mathbf{G}_r (\mathbf{m} - \mathbf{m}^{ref})\|_1. \quad (8)$$

The L_1 norm is used to encourage sparsity in the model parameters. The Sparse regularization term penalizes the absolute values of the elements of $\mathbf{W}_r \mathbf{V}_r \mathbf{G}_r (\mathbf{m} - \mathbf{m}^{ref})$ instead of their squared values, promoting sparsity in the solution [11]. The final objective functions for two types of the gravity inversions are expressed in Eqs.9 and 10.

$$\min \phi(m)_{Tikhonov} = \|\mathbf{G}\mathbf{p} - \mathbf{d}^{obs}\|_2^2 + \beta \sum_{r=s,x,y,z} \alpha_r \|\mathbf{W}_r \mathbf{V}_r \mathbf{G}_r (\mathbf{m} - \mathbf{m}^{ref})\|_2^2. \quad (9)$$

$$\min \phi(m)_{sparse} = \|\mathbf{G}\mathbf{p} - \mathbf{d}^{obs}\|_2^2 + \beta \sum_{r=s,x,y,z} \alpha_r \|\mathbf{W}_r \mathbf{V}_r \mathbf{G}_r (\mathbf{m} - \mathbf{m}^{ref})\|_1. \quad (10)$$

By equating the gradient of the objective function to zero, $\nabla \phi(m) = 0$, we can derive the solutions for both inversion cases, representing the recovered models [26]. These solutions are expressed in Eqs.11 and 12.

$$\mathbf{m}_{Tikhonov} = (\mathbf{G}^T \mathbf{W}_d^T \mathbf{W}_d \mathbf{G} + \beta \mathbf{W}_m^T \mathbf{W}_m)^{-1} (\mathbf{G}^T \mathbf{W}_d^T \mathbf{W}_d \mathbf{d}^{obs} + \beta \mathbf{W}_m^T \mathbf{m}^{ref}). \quad (11)$$

$$\mathbf{m}_{sparse} = (\mathbf{G}^T \mathbf{W}_d^T \mathbf{W}_d \mathbf{G} + \beta \mathbf{W}_m^T \text{diag}(\mathbf{R}) \mathbf{W}_m)^{-1} * (\mathbf{G}^T \mathbf{W}_d^T \mathbf{W}_d \mathbf{d}^{obs} + \beta \mathbf{W}_m^T \mathbf{m}^{ref}). \quad (12)$$

$\text{diag}(\mathbf{R})$ is a diagonal matrix imposing the iteratively updated weights [26-29]. The choice between these regularization techniques influences the characteristics of the recovered model. Tikhonov tends to produce smooth solutions, while Sparse encourages sparsity in the solution.

3. Synthetic scenarios

In geophysical exploration, the choice of the regularization method can significantly impact the quality and accuracy of inversion results. To illustrate this, we conducted a study in a homogeneous half-space using forward modelling to investigate the effectiveness of both Tikhonov and Sparse regularization in recovering simple subsurface features. For the first synthetic model, we discretized the synthetic environment with dimensions of 200m \times 200m \times 100m into 80 \times 80 \times 40 cells. The x-axis interval ranges from 0 to 200m, the y-axis interval spans from -100m to 100m, and the z-axis interval extends from -100m to 0. We present both synthetic models in Slice 40 at $y = 0$, indicating that the figures represent an x-z cross-section at $y = 0$, corresponding to the indexed Slice 40. Within this environment, we created a simple cube (Figure 2.a) with the dimensions of 40m \times 40m \times 40m, which was embedded in the homogeneous background with zero density contrast. The density contrast for the synthetic cube was considered as 1.2 g/cm³. The observed gravity anomalies are added with 2% Gaussian random noise in both synthetic models. The objective was to accurately recover the properties of this cube, such as its geometry, density, and depth using the gravity inversion methods. Our findings revealed notable differences between two regularization methods. When employing the Sparse regularization,

the results were remarkably accurate, yielding a model that closely resembled the true properties of the cube. The sparse (L_1) regularization, also known as Lasso, is renowned for promoting sparsity in the solution vector. It encourages the model to identify and highlight the essential features within the data. In this case, it accurately illustrates the cube's dimensions and depth (Figure 2.b). In contrast, the Tikhonov regularization (Figure 2.c) yielded a smoother model that struggled to recover the true depth of the cube.

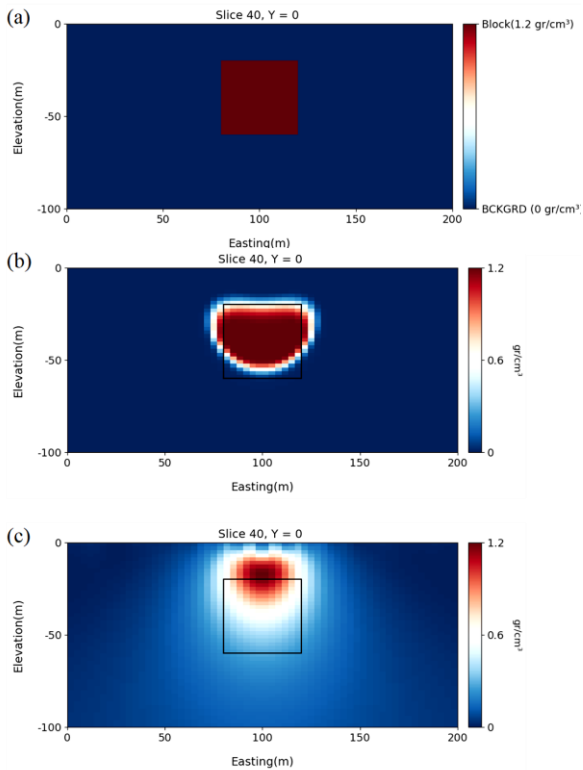


Figure 2. The synthetic data modelling for a single rectangular cube, (a) the true density model, (b) the result of inversion by the Sparse regularization, (c) the result of inversion by the Tikhonov regularization.

The Tikhonov regularization is designed to encourage solutions where all model parameters are small, but not necessarily sparse. This tendency toward smoothness can sometimes blur the sharp boundaries of subsurface features, making it challenging to precisely locate the depth of the cube. Figure 3a illustrates the observed anomalies resulting from the true model, and Figures 3b and 3d depict the observed anomalies resulting from inversions with the Sparse and Tikhonov regularization, respectively. The normalized misfit values further reinforced these observations; with the Sparse regularization achieving a lower misfit of around 1 (Figure 3.c), indicating a better fit to the observed data. On the other hand, the Tikhonov regularization resulted in a higher misfit of around 1.5 (Figure 3.e), suggesting a less accurate fit.

The selection of a regularization method should be approached with careful consideration, taking into account the specific objectives and characteristics of the inversion problem. This choice plays a crucial role in shaping the interpretation of geophysical data. The cross-plot of inversion results for the first synthetic model is depicted in Figure 4, showcasing the correlation between inversion results. In a straightforward explanation, each point on cross-plots corresponds to a cell in the discretized environment. After distinct inversions with various regularization terms, each cell now represents two density contrasts. One arises from an inversion with the sparsity regularization, while the other stems from an inversion with the Tikhonov regularization. In these types of plots, we employ cross-correlation to

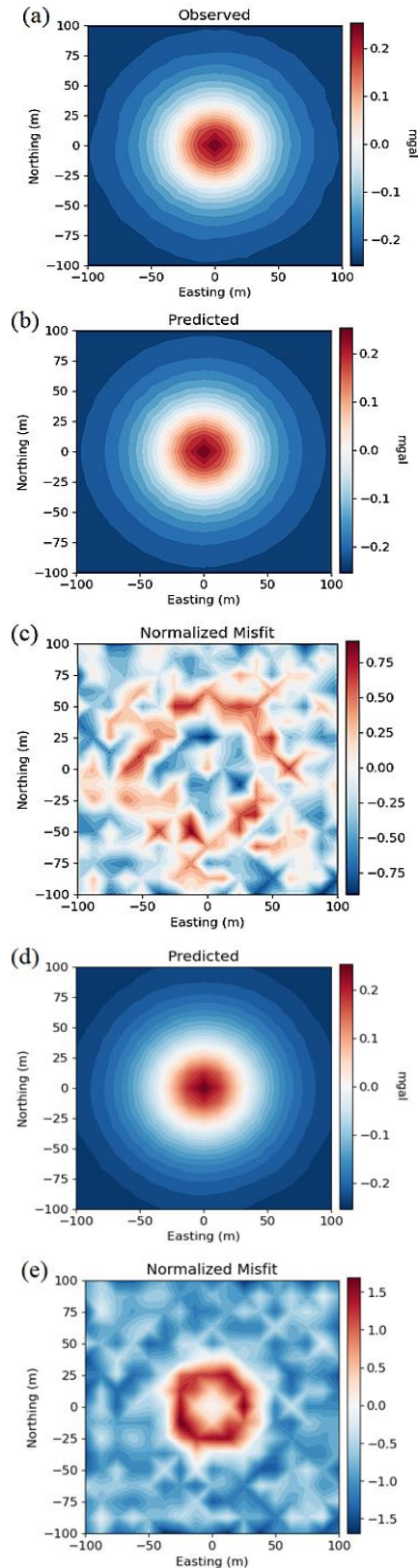


Figure 3. (a) The observed data from the true model, (b) the predicted data from inversion with the Sparse regularization, (c) the normalized misfit for the gravity inversion with the Sparse regularization, (d) the predicted data from inversion with the Tikhonov regularization, (e) normalized misfit for the gravity inversion with the Tikhonov regularization.

In Figures 4 and 7, we use the (+) signs to represent the density contrast of background and objects, illustrating the efficiency of each inversion method in reconstructing them. For the first synthetic model, 15 iterations are employed in the gravity inversion with the Sparse regularization and the Tikhonov regularization undergoes 10 iterations.

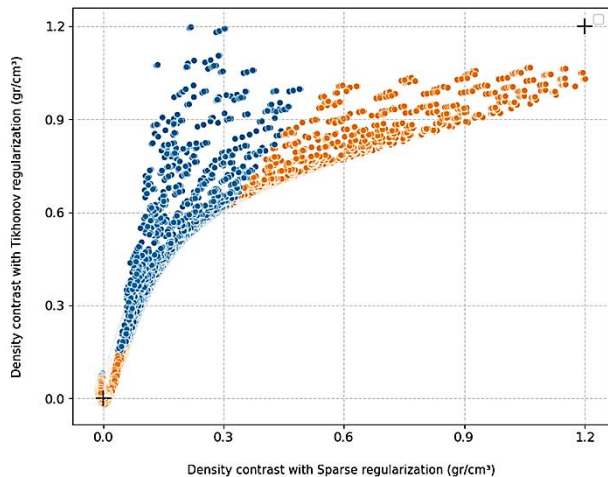


Figure 4. The cross-plot for the first synthetic model.

For the second model, we introduced a synthetic configuration consisting of two rectangular cubes with distinct densities (Figure 5.a) with the dimension of $40\text{m} \times 20\text{m} \times 20\text{m}$. The left rectangular cube has a density contrast of 1 g/cm^3 , and the right rectangular cube has a density contrast of 1.5 g/cm^3 , with the background density set to zero. Both rectangular cubes were positioned at the same depth and separated by a distance of approximately 70 meters. Utilizing the Sparse regularization yielded highly promising inversion results. The estimated depths for each geometrical shape closely approximated the true model, and the geometry of both cubes within the recovered model closely resembled reality (Figure 5.b). In contrast, the application of the Tikhonov regularization resulted in a smoother but somewhat misleading model. While achieving a desirable overall smoothness, it struggled to accurately recover the depths and dimensions of the cubes. Notably, the cube with a lower density posed a particular challenge for the Tikhonov regularization method, highlighting its limitations in preserving sharp boundaries and specific details of subsurface features (Figure 5.c). The inversion with the Sparse regularization involved 15 iterations, while the inversion with the Tikhonov regularization utilized 10 iterations. The application of the iteratively reweighted least squares (IRLS) method in the first inversion heightened the algorithm's sensitivity to depth, resulting in a more accurate recovery of the buried structures.

Figure 6a represents the observed anomalies resulting from the true model. Figures 6b and 6d represent the observed anomalies resulting from the Sparse and Tikhonov regularization, respectively. In a short explanation, "misfit" refers to the quantitative measure of the difference between observed data and the data predicted by a model. It is a key parameter used to evaluate how well the model reproduces the actual measurements. The normalized misfit values obtained from inversion methods for the second synthetic model are presented in Figure 6. Notably, we achieved a significantly more favorable misfit using the Sparse regularization (Figure 6c) compared to the Tikhonov regularization (Figure 6e).

This indicates a superior data fit with the Sparse regularization, showing its effectiveness in capturing the underlying subsurface structures. In Figure 7, our cross-plot of the inversion results for the second synthetic model provides a visual representation of the differences in performance between two regularization techniques. The orange and blue data points adhere to the same pattern observed in the first synthetic model. This plot conveys information about the density contrast trend in two inversion conditions. As evident, similar to the first synthetic model,

sparsity regularization demonstrates a superior ability to distinguish main objects from the background. The distribution of the blue points indicates that cells with higher density contrast in inversion using the L_2 norm exhibit lower density contrast in inversion with the sparsity regularization. This suggests that the obtained sources' depth and density distributions within these cells are not the same. Furthermore, taking into account the variation in density contrast, it becomes apparent that inversion with the sparsity regularization was more effective in capturing the properties of the second cube with lower density contrast compared to inversion with the Tikhonov regularization.

In conclusion, in both synthetic models, the Sparse regularization demonstrates an advantage over the Tikhonov regularization in reconstructing geometry and true depth. Additionally, a more effective separation between background and objects is achieved through inversion with the sparsity regularization. However, the benefits of the Tikhonov regularization become evident when dealing with noisy data, an aspect that will be discussed in section 4.

4. Application to the real data

4.1 Geological Context

The Safu deposit in Iran is a significant manganese deposit situated in the Khoy area, and its geological context is rooted in the Late Jurassic to the Late Cretaceous period. This deposit is a product of the mature back-arc spreading that characterized the Khoy-Zanjan area during this time. The Late Jurassic to the Late Cretaceous period witnessed extensive back-arc spreading events in various regions, including the Khoy-Zanjan area in the north Sanandaj-Sirjan zone. The Safu deposit, being an ophiolite-hosted manganese deposit, formed within this geological setting, specifically in the Khoy area. The ore formation in the Safu is associated with mature back-arc spreading, a tectonic environment marked by the extension of the Earth's crust behind a subduction zone. This deposit is classified as an ophiolite-hosted manganese deposit, signifying its connection to ophiolitic belts formed in oceanic environments [30].

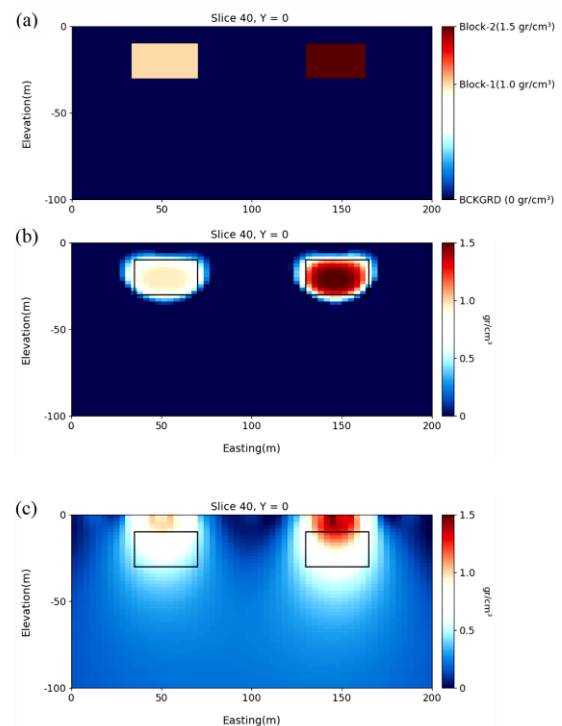


Figure 5. The synthetic data modelling for two rectangular cubes, (a) the true density model, (b) the result of inversion by the Sparse regularization (c) result of inversion by the Tikhonov regularization.

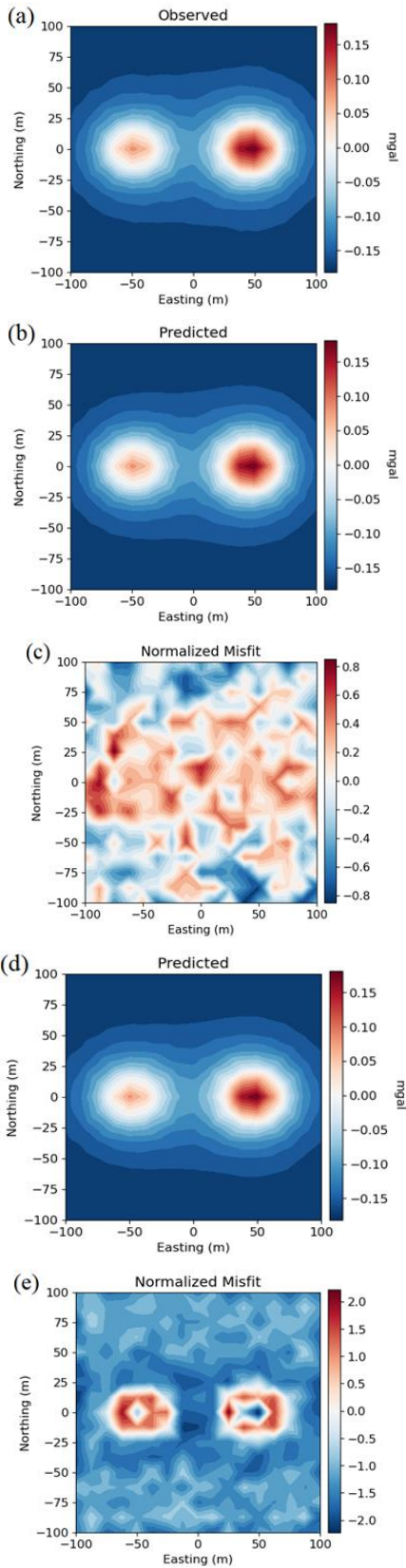


Figure 6. Observed data from true model, (b) predicted data from inversion with the Sparse regularization, (c) normalized misfit for the gravity inversion with Sparse regularization, (d) predicted data from inversion with Tikhonov regularization, (e) normalized misfit for the gravity inversion with Tikhonov regularization

Chronologically, the Safu deposit took shape during the Late Cretaceous, a period marked by significant geological events, including the Laramide Orogeny and intense deformation. Manganese mineralization in the Safu is linked to ore interlayers, particularly with reddish radiolarites that are younger than the Middle Jurassic. Geochemical studies emphasize the supra-subduction nature of ophiolites, including those hosting manganese deposits, such as the Safu [30]. These ophiolites developed in intra-oceanic island arc environments during the Late Triassic to the Late Cretaceous. Geological and geochemical evidence suggests that the deposition of ores resulted from submarine hydrothermal solutions on the floor of the Neo-tethys ocean basin during the Upper Cretaceous [31].

The Mn/Fe ratios in this deposit exhibit variability, with the average ratio several times higher than the values found in metal-bearing sediment deposits of mid-ocean ridges. High Mn/Fe and Si/Al ratios, coupled with low quantities of rare metals, particularly nickel (Ni), cobalt (Co), and copper (Cu), limited amounts of cerium (Ce) elements, and elevated levels of silicon dioxide (SiO₂), barium (Ba), iron (Fe), manganese (Mn), and strontium (Sr), serve as the evidence of the enrichment and depletion of manganese from submarine hydrothermal fluids. The role of hydrogenation processes in the formation of this deposit appears to be insignificant [32].

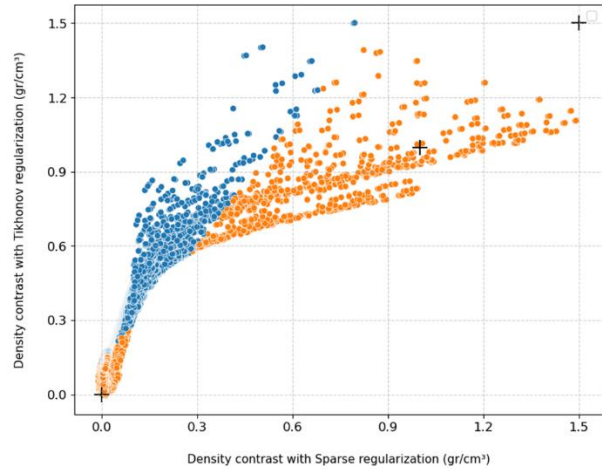


Figure 7. The cross-plot for the second synthetic model.

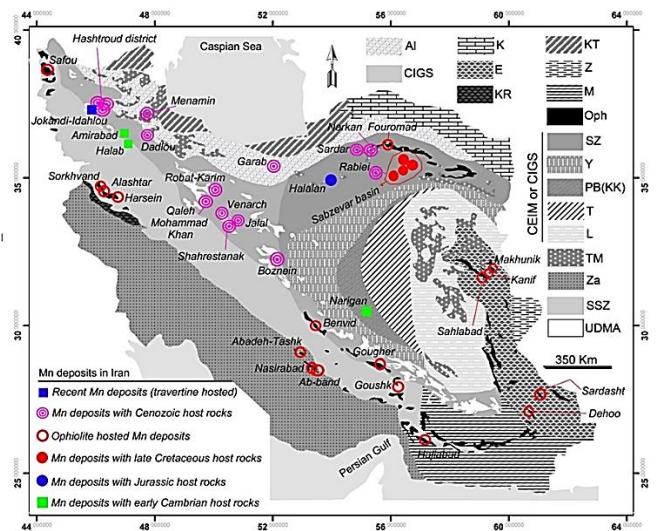


Figure 8. The distribution map of manganese deposits according to the age of host rocks within the main tectonic elements of Iran [30].

4.2. Gravity Data

For the gravity survey, a CG3 gravimeter with a precision of 5 microgal was utilized. The data collection phase involved a network of 601 sampling points, with station spacing ranging from 5 to 10 meters [31]. In the northeastern corner of the survey area, fewer gravity data points were collected due to the rugged topography. Following gravity correction, regional trends were eliminated using a first-order polynomial fitting method [33]. In Figure 9, we present the residual gravity anomaly (Figure 9a) and the 20m upward continuation of gravity data (Figure 9b). Notably, a linear sharp anomaly is discernible in the central region of the survey area, reaching a maximum value of approximately 3 mgal. Profiles A-B and C-D depict the sections where the inversion results are displayed.

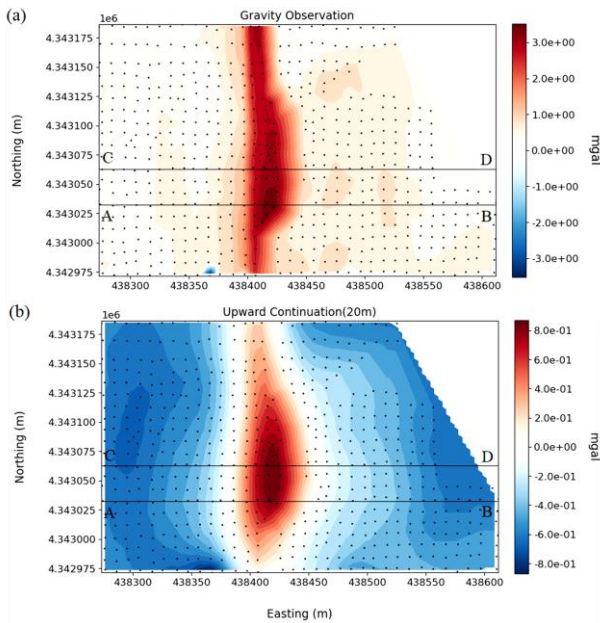


Figure 9. (a) Residual gravity anomaly, (b) upward continuation (20m) of gravity data.

4.3. Inversion results

To conduct the real data inversion, we discretized the subsurface environment using a grid of $80 \times 60 \times 20$ cells. The outcomes of the inversion of gravity data are illustrated along two profiles (A-B and C-D), as shown in Figure 9. About 25 iterations were undertaken for the inversion with the Sparse regularization, and 10 iterations were carried out for inversion with the Tikhonov regularization. The density limits for both inversions were set between 2.0 g/cm^3 and 4.5 g/cm^3 , with a background density considered as 2.6 g/cm^3 . Figure 10 depicts the results of the gravity inversion along the A-B and C-D profiles. In Figures 10a and 10c, the inversion results with the Sparse regularization reveal the presence of an anomalous target at approximately 5 meters deep, with sharp boundaries delineating the massive target. Figures 10b and 10d display the inversion results with the Tikhonov regularization, showcasing a smoother model characterized by gradual changes in density contrast. Both models indicate a shallow top depth, highlighting the evident near-surface location of the ore. By moving to the northern part of the survey area, we observed a slight increase in the depth of the anomalous target, accompanied by more gradual changes in the inversion results (Figures 10b and 10d).

We additionally present the inversion results along the Z-direction at a depth of 20 meters in Figure 11. Both inversion methods (11a and 11b) unveil a linear mineralization with a concentration in the lower section of the survey area. As indicated by the inversion results, the mineral deposit is situated at depths ranging from 5 to 25 meters, implying a

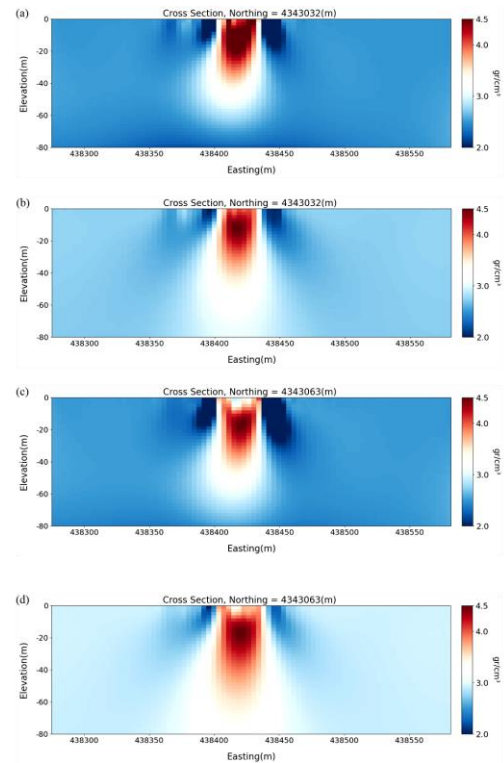


Figure 10. (a) The inversion result along A-B profile with the Sparse regularization, (b) Inversion result along A-B profile with the Tikhonov regularization, (c) Inversion result along C-D profile with the Sparse regularization, (d) Inversion result along C-D profile with the Tikhonov regularization.

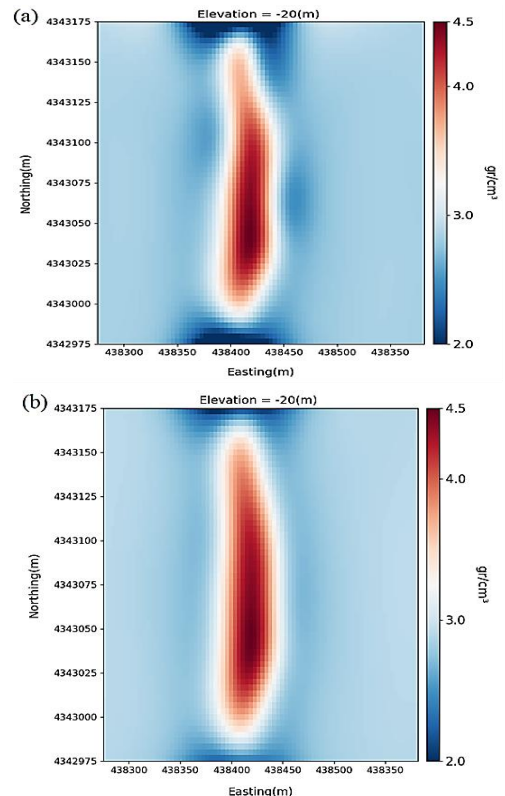


Figure 11. (a) Inversion result along Z direction with Sparse regularization, (b) Inversion result along Z direction with the Tikhonov regularization.

superficial target. It is evident that the Tikhonov regularization is more effective in mitigating the presence of noise at the edges of the survey area compared to the Sparse regularization.

We illustrate the normalized misfits of inversions in Figure 12. Figures 12a and 12c depict the predicted data from the gravity inversion with the Sparse and Tikhonov regularization, respectively. It is noteworthy to mention that elevated misfit values are observed in the real data inversion, as evident in Figures 12b and 12d. This is primarily attributed to the challenges posed by Limited Data Coverage at the edges of the survey area, where inversion encounters difficulties in providing accurate results. Insufficient data points in these regions give rise to information gaps and reduced data coverage, thereby yielding incomplete and less reliable subsurface models. Notably, when we concentrate on the primary anomalous location, we observe lower and acceptable misfit values for both inversion methods.

In Figure 13, we display a cross-plot of the real data inversion, effectively illustrating the trade-off between sparsity and smoothness. In simpler terms, it serves as the representation of 'Sparsity vs. Smoothness.' Similar to the synthetic modelling, the blue color represents data where the Tikhonov regularization resulted in a higher density contrast than the Sparse regularization, while the orange color signifies cases where the Sparse regularization produced a higher density contrast than the Tikhonov regularization. A nearly linear relationship between the inversion results indicates that both methods are effective, providing consistent results for the manganese ore. There is a vertical distribution of the density contrast at the beginning and end of the cross-plot. This implies that the lowest and highest density contrasts obtained through inversion with the sparsity regularization exhibit a gradual change in the other reconstructed model, emphasizing a smooth density model resulting from inversion with the Tikhonov regularization. However, in contrast to the synthetic models, inversion with the Tikhonov regularization demonstrates an acceptable performance in real cases. This distinction becomes evident when comparing the cross-plot of real cases with that of synthetic models. The term "acceptable" means that both inversion methods result in a closely similar density model.

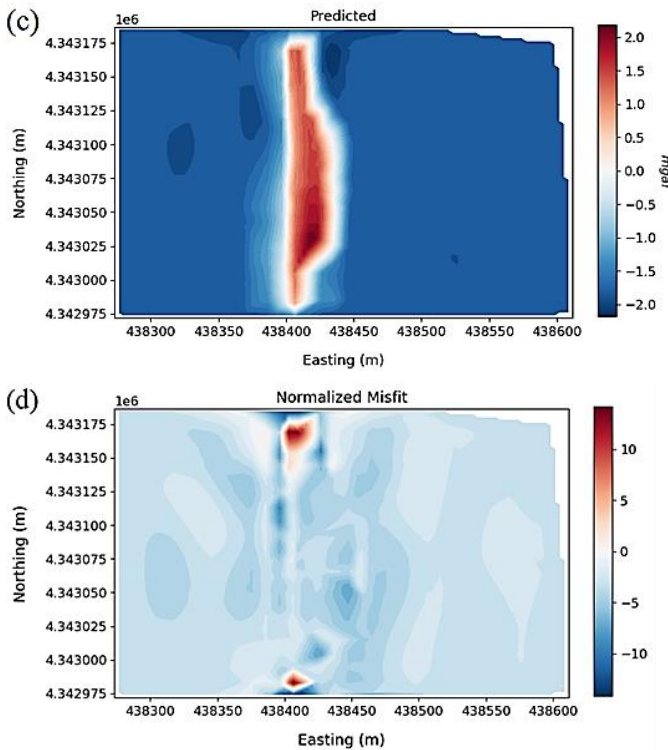


Figure 12. (a) predicted data from inversion with Sparse regularization, (b) normalized misfit for the gravity inversion with The Spare regularization, (c) predicted data from inversion with the Tikhonov regularization, (d) normalized misfit for the gravity inversion with the Tikhonov regularization.

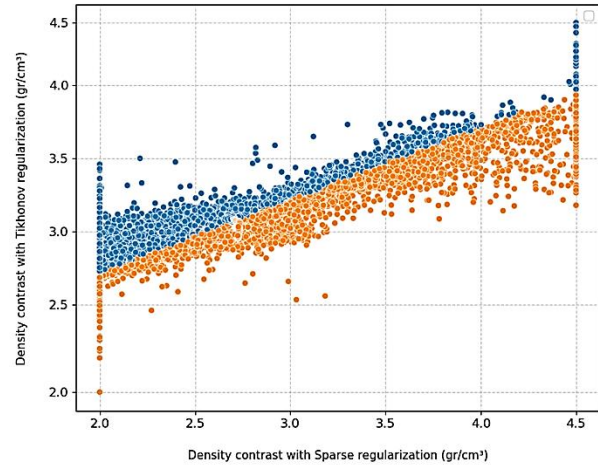


Figure 13. The cross-plot for the real gravity data.

5. Conclusion

In this study, we conducted an extensive comparative analysis of two prominent regularization methods: Sparse and Tikhonov. Our focus was on their effectiveness in recovering ore deposits. To ensure a robust assessment, we began by applying these methods to synthetic geometric shapes. This provided a controlled setting for evaluating their performance. Subsequently, we extended our investigation to real gravity data, simulating practical scenarios. This approach allowed us to assess how well the Sparse and Tikhonov regularization techniques could handle the complexities of actual geological settings. The results highlighted the capabilities and limitations of each method. The Sparse regularization proved proficient at capturing sparse and sharp features, making it suitable for identifying distinct ore deposits. The Tikhonov regularization, on the other hand, demonstrated excellence in producing smoother, more gradual models, ideal for characterizing broader geological structures. Our research offers valuable insights for geophysical exploration, revealing the complex interaction between regularization techniques and their suitability for specific geological scenarios.

Acknowledgments

We would like to express our sincere gratitude to the University of Tehran, Faculty of Mining Engineering, for their invaluable support. We are also thankful to the faculty members of the Institute of Geophysics, university of Tehran, for their guidance and feedback, which contributed to the quality of this research. Finally, Prof. Ebrahimzadeh Ardestani is also appreciated for data provision.

REFERENCES

- [1] Wang, Y., Leonov, A. S., Lukyanenko, D. V., & Yagola, A. G. (2020). General Tikhonov Regularization with Applications in Geoscience. *CSIAM Transactions on Applied Mathematics*, 1(1), 53–85.
- [2] Tarantola, A. (2005). *Inverse Problem Theory and Methods for Model Parameter Estimation*. Society for Industrial and Applied Mathematics (SIAM). (p. 168).
- [3] Jordi, C., Doetsch, J., Günther, T., Schmelzbach, C., & Robertsson, J. O. A. (2018). Geostatistical regularization operators for geophysical inverse problems on irregular meshes. *Geophysical Journal International*, 213(2), 1374–1386.

- [4] Menke, W., & Eilon, Z. (2015). Relationship between Data Smoothing and the Regularization of Inverse Problems. *Pure and Applied Geophysics*, 172, 2711-2726.
- [5] Aster, R. C., Borchers, B., & Thurber, C. H. (2019). *Parameter Estimation and Inverse Problems* (3rd ed.). Elsevier.
- [6] Silva, J. B. C., Medeiros, W. E., & Barbosa, V. C. F. (2001). Potential-field inversion: Choosing the appropriate technique to solve a geologic problem. *Geophysics*, 66(2), 511-520.
- [7] Hong, B. W., Koo, J. K., Dirks, H., & Burger, M. (2017). Adaptive Regularization in Convex Composite Optimization for Variational Imaging Problems. *Lecture Notes in Computer Science*, 10496, 268-280.
- [8] Tikhonov, A. N., & Arsenin, V. Y. (1977). *Solutions of Ill-posed Problems*. V.H. Winston and Sons, Washington, DC.
- [9] Tousemalani, R., & Saibi, H. (2015). 3D Gravity Inversion using Tikhonov Regularization. *Acta Geophysica*, 63, 1044-1065.
- [10] Fernández-Martínez, J. L., Pallero, J. L. G., Fernández-Muñiz, Z., & Pedruelo-González, L. M. (2014). The effect of noise and Tikhonov's regularization in inverse problems. Part I: The linear case. *Journal of Applied Geophysics*, 108, 176-185.
- [11] Gholami, A., & Siahkoochi, H. R. (2010). Regularization of linear and non-linear geophysical ill-posed problems with joint sparsity constraints. *Geophysical Journal International*, 180(2), 871-882.
- [12] Grasmair, M., Haltmeier, M., & Scherzer, O. (2015). Sparsity in Inverse Geophysical Problems. In W. Freeden, M. Nashed, & T. Sonar (Eds.), *Handbook of Geomathematics* (p. 1680). Springer
- [13] Lin, Y., & Huang, L. (2015). Quantifying subsurface geophysical properties changes using double-difference seismic-waveform inversion with a modified total-variation regularization scheme. *Geophysical Supplements to the Monthly Notices of the Royal Astronomical Society*, 203(3), 2125-2149.
- [14] Strong, D., & Chan, T. (2003). Edge-preserving and scale-dependent properties of total variation regularization. *Inverse problems*, 19(6), S165.
- [15] Du, Z., Liu, D., Wu, G., Cai, J., Yu, X., & Hu, G. (2021). A high-order total-variation regularization method for full-waveform inversion. *Journal of Geophysics and Engineering*, 18(2), 241-252.
- [16] Lima, W. A., Martins, C. M., Silva, J. B., & Barbosa, V. C. (2011). Total variation regularization for depth-to-basement estimate: Part 2 — Physicogeologic meaning and comparisons with previous in-version methods. *GEOPHYSICS*, 76, I13-I20.
- [17] Sen, M. K., & Stoffa, P. L. (2013). *Global Optimization Methods in Geophysical Inversion*. Cambridge University Press. (p. 37)
- [18] Villalon-Turrubiates, I. E., & Herrera-Nuñez, A. (2009). Performance study of the robust bayesian regularization technique for remote sensing imaging in geophysical applications. *Mexican International Conference on Computer Science* (pp. 3-12).
- [19] Vatankhah, S., Ardestani, V. E., & Renaut, R. A. (2014). Automatic estimation of the regularization parameter in 2D focusing gravity inversion: application of the method to the Safo manganese mine in the northwest of Iran. *Journal of Geophysics and Engineering*, 11(4), 045001.
- [20] Varfinezhad, R., & Ardestani, V. (2021). 2D inversion of gravity data including depth weighting and compactness constraints: a case study on the data set of the manganese mine of Safo. 19th Iranian Geophysical Conference—November, 2020 (pp. 152-156).
- [21] Cockett, R., Kang, S., Heagy, L. J., Pidlisecky, A., & Oldenburg, D. W. (2015). SimPEG: An open source framework for simulation and gradient-based parameter estimation in geophysical applications. *Computers & Geosciences*, 85, 142-154.
- [22] Ardestani, V. E. (2023). Sparse norm and cross-gradient inversions of gravity and magnetic data sets utilizing open-source resources in Python: Case study of hematite ore body in Jalal Abad area (Iran). *Journal of the Earth and Space Physics*.
- [23] Pluff, D., (1976). Gravity and Magnetic fields of polygonal prisms and application to magnetic terrain corrections. *Geophysics*, 41, 727-41.
- [24] De Breaecker, J. Cl. (1966). On: "The gravitational attraction of a right rectangular prism," by Dezsö Nagy (*Geophysics*, April, 1966, pp. 362-371). *Geophysics*, 31, 987-987.
- [25] Li, Y., & Oldenburg, D. W. (1996). 3-D inversion of magnetic data. *Geophysics*, 61, 394-408.
- [26] Oldenburg, D. W., & Li, Y. (2005). Inversion for applied geophysics: A tutorial. *Investigations in Geophysics*, 89-150.
- [27] Abedi, M., Gholami, A., & Norouzi, G.H. (2014). A new stable downward continuation of airborne magnetic data based on Wavelet deconvolution. *Near Surface Geophysics*, 12, 751-762.
- [28] Abedi, M., Gholami, A., & Norouzi, G.H. (2014). 3D inversion of magnetic data seeking sharp boundaries: a case study for a porphyry copper deposit from Now Chun in central Iran. *Near Surface Geophysics*, 12, 657-666.
- [29] Abedi, M. (2019). AIRRLS: An Augmented Iteratively Re-weighted and Refined Least Squares Algorithm for Inverse Modeling of Magnetometry Data. *Journal of Geological Research*, 1, 16-27.
- [30] Maghfouri, S., Rastad, E., Movahednia, M., Lentz, D. R., Hosseinzadeh, M. R., Ye, L., & Mousivand, F. (2019). Metallogeny and temporal-spatial distribution of manganese mineralizations in Iran: Implications for future exploration. *Ore Geology Reviews*, 115, 103026.
- [31] Soltanabadi, R., & Ardestani, V. E. (2018). 3D inversion of gravity data of Safo mining site using linear programming and simplex algorithm. *Journal of Research on Applied Geophysics*, 4(1), 137-155.
- [32] Imamalipour, A. (2005). Geochemistry, mineralogy, and origin of Safu manganese deposit. 9th Meeting of Geological Society of Iran (pp. 256-269).
- [33] Beltrão, J. F., Silva, J. B. C., & Costa, J. C. (1991). Robust polynomial fitting method for regional gravity estimation. *GEOPHYSICS*, 56, 80-89.